

PCCP

Accepted Manuscript



This is an *Accepted Manuscript*, which has been through the Royal Society of Chemistry peer review process and has been accepted for publication.

Accepted Manuscripts are published online shortly after acceptance, before technical editing, formatting and proof reading. Using this free service, authors can make their results available to the community, in citable form, before we publish the edited article. We will replace this *Accepted Manuscript* with the edited and formatted *Advance Article* as soon as it is available.

You can find more information about *Accepted Manuscripts* in the [Information for Authors](#).

Please note that technical editing may introduce minor changes to the text and/or graphics, which may alter content. The journal's standard [Terms & Conditions](#) and the [Ethical guidelines](#) still apply. In no event shall the Royal Society of Chemistry be held responsible for any errors or omissions in this *Accepted Manuscript* or any consequences arising from the use of any information it contains.

Photodissociation dynamics of ethanethiol in clusters: Complementary information from velocity map imaging, mass spectrometry and calculations[†]

Pavla Svrčková,^{a,b} Andriy Pysanenko,^a Jozef Lengyel,^{a,b} Peter Rubovič,^a Jaroslav Kočíšek,^a Viktoriya Poterya,^a Petr Slavíček,^{a,b} and Michal Fárník^{*a}

Received Xth XXXXXXXXXXXX 20XX, Accepted Xth XXXXXXXXXXXX 20XX

First published on the web Xth XXXXXXXXXXXX 2015

DOI: 10.1039/b000000x

We investigate the solvent effects on photodissociation dynamics of S–H bond in ethanethiol CH₃CH₂SH (EtSH). The H fragment images are recorded by velocity map imaging (VMI) at 243 nm in various expansion regimes from isolated molecules to clusters of different size and composition. The VMI experiment is accompanied by electron ionization mass spectrometry using a reflectron time-of-flight mass spectrometer (RTOFMS). The experimental data are interpreted with *ab initio* calculations. The direct S–H bond fission results in a peak of fast fragments at $E_{kin}(H) \approx 1.25$ eV with a partly resolved structure corresponding to vibrational levels of the CH₃CH₂S cofragment. Clusters of different nature from dimers to large (EtSH)_N, $N \geq 10$ clusters and to ethanethiol clusters embedded in larger argon “snowballs” are investigated. In the clusters a sharp peak of near-zero kinetic energy fragments occurs due to the *caging*. The dynamics of the fragment caging is pictured theoretically, using multi-reference *ab initio* theory for ethanethiol dimer. The larger cluster character is revealed by the simultaneous analysis of the VMI and RTOFMS experiments; none of these tools alone can provide the complete picture.

1 Introduction

The sulphur compounds are important players in aerosol generation and in atmospheric chemistry in general.¹ The ultraviolet (UV) photolysis of various sulphur containing molecules is a key part of the sulphur cycle in the atmosphere. The detailed investigations of the S–H bond photodissociation dynamics in molecules and clusters thus contributes to the understanding of atmospheric sulphur (photo)chemistry.

In our work, we focus on the photodissociation of ethanethiol CH₃CH₂SH (EtSH). Based on the analogy with methanethiol, two reaction channels are expected in the spectral region above 200 nm, the S–H and S–C bond breaking:



The present experiment focuses on the S–H bond fission, and

[†] Electronic Supplementary Information (ESI) available: H-fragment velocity map images, mass spectra from different ethanethiol clusters, and calculated cluster structures. See DOI: 10.1039/b000000x/

^a J. Heyrovský Institute of Physical Chemistry v.v.i., Academy of Sciences of the Czech Republic, Dolejškova 3, 18223 Prague, Czech Republic. Fax: +4202 8658 2307; Tel: +4202 6605 3206; E-mail: michal.farnik@jh-inst.cas.cz

^b Department of Physical Chemistry, University of Chemistry and Technology Prague, Technická 5, Prague 6, Czech Republic.

we primarily investigate the solvent effects on photodynamics in different types of clusters.

So far, the EtSH molecule photochemistry was characterized rather incompletely from an experimental point of view. Even the full UV absorption spectrum was not recorded and the UV absorption cross sections were published only for several wavelengths.^{2,3} The velocity map imaging⁴ (VMI), which is the up-to-date method to investigate the photodissociation dynamics,⁵ was used only once to study the S–H photodissociation of EtSH at 243 nm previously.⁶ This rather limited information contrasts with the number of studies of the analogical methanethiol molecule which was the subject of numerous experimental^{7–15} and theoretical investigations.^{14–21} From these studies, the following picture emerged for methanethiol photochemistry. The absorption around 240 nm (corresponding to the population of the 1A'' electronic state) leads almost exclusively to the S–H bond rupture. This channel remained dominant even upon the excitation into the 2A'' below 220 nm, yet the C–S dissociation channel was observed too. The dissociation was very fast, leading to the high anisotropy of the photofragments.

In relevance to the present mass spectrometry of EtSH clusters, a mass spectrometric study of the molecule should be mentioned.²² More recently the ionization energy and conformational isomers were revealed using nonresonant two-photon pulsed field ionization photoelectron spectroscopy,²³

and vacuum ultraviolet mass-analyzed threshold ionization spectroscopy.²⁴

Here, we investigate the photochemistry of EtSH by VMI, and cluster structure and composition by electron ionization RTOFMS. We provide new data for the S–H photodissociation in the isolated EtSH molecule at 243 nm with partly resolved vibrational structure. Our experiment also reveals the origin of the previously observed slow H-fragments⁶ as a consequence of multiphoton processes. Then we focus on the photodissociation of ethanethiol in different clusters, ranging from dimers to large (EtSH)_N clusters, and to ethanethiol clusters embedded in larger argon clusters. The detailed photodissociation dynamics is rationalized by *ab initio* calculations for the isolated molecule as well as for clusters.

2 Experiment

The experiments were carried out on the CLUster Beam (CLUB) apparatus which is a very versatile molecular beam setup.^{25–29} In the present study we exploited two of the possible different experiments: the VMI and electron ionization RTOFMS.

To generate the beam of the molecules or clusters the carrier gas (He or Ar) was passed through a reservoir filled with liquid EtSH. The reservoir was placed outside the vacuum, and kept at a constant temperature T_R by heating it resistively in the mixture of CO₂ ice and ethylene glycol. The EtSH vapour was transported by the carrier gas at a stagnation pressure P_0 towards a nozzle kept at the temperature $T_0 \approx 313$ K, and expanded into vacuum. Helium was used as the buffer gas for generating isolated molecules and small clusters up to trimers, while the larger (EtSH)_N, $N \geq 10$, clusters and Ar-covered species were generated in coexpansions with argon. Table 1 summarizes the expansion conditions.

Table 1 Expansion conditions. “Cluster size n ” denotes the largest (EtSH)_n⁺ fragment discernible in the mass spectra; “*mix*” corresponds to the appearance of Ar_m(EtSH)_n⁺ fragments in the mass spectra; the arrows indicate a gradual change in the parameter. The nozzle parameters: diameter $d = 50$ μm , opening angle $\alpha = 30^\circ$, length $l = 2$ mm.

Buffer gas	Stagnation pressure P_0 (bar)	Reservoir temperature T_R (K)	Concentration C (%)	Cluster size n
He	1	222	1.2	1
	2,3	263	7.5,5	3
Ar	2	263	7.5	15
	2→5	276	14→6	13–15
	5	263→220	3→0.2	17→ <i>mix</i>

2.1 Velocity map imaging

The cluster beam was skimmed and passed through two differentially pumped chambers before entering the chamber hosting the VMI assembly mounted perpendicularly to the beam axis. The molecules and clusters interact with the laser in the center of an electrostatic lens system which extracts the ionized photoproducts towards a position sensitive detector 50 cm upwards from the interaction point. The imaging system design follows approximately the original VMI of Eppink and Parker.⁴ The detector (two multichannel plates with 56 mm diameter in Chevron configuration and the phosphor screen) was operated in gated mode which enabled imaging of a single ion mass. The gating was triggered by a laser light pulse delayed using a delay generator (BNC 575).

Laser radiation at 243.1 nm was used to dissociate the EtSH molecules and REMPI ionize the H-atoms. The tunable UV radiation was generated by doubling the 630 nm output of the dye laser (Pulsare-S, Fine Adjustment) pumped by the second harmonics (532 nm) of the Nd:YAG laser (Spotlight 1500, Innolas). The 315 nm was frequency summed with the fundamental 1064 nm of the Nd:YAG laser. The lasers were operated at a 10 Hz frequency in nanosecond regime. The laser beam was focussed with a 700 mm lens onto a spot of a radius ≈ 24 μm in the interaction region. The laser radiation was polarized so that the electric field vector of the radiation was parallel to the molecular beam, i.e. perpendicular to the imaging TOF axis. To investigate multiphoton processes the energy at the laser output was varied between 1.2 and 4.4 mJ/pulse corresponding to the photon fluxes at the interaction region between 10^{27} and 10^{28} photons·cm⁻²·s⁻¹ (using different output power and neutral density filters).

The images were recorded with an 16-bit greyscale CCD camera (unibrain Fire-i 780b) with the imaging lens (25 mm, $f/1.6$), connected to an acquisition computer via a FireWire interface and controlled by a custom made program. To process the images several reconstruction methods were used to check the consistency of our results: the inverse Abel transform and Hankel method,³⁰ Iterative Inversion method,³⁰ and the BASEX.³¹ Comparing different evaluation methods was important especially for the search for a narrow zero-kinetic-energy (zero-KE) peak due to the fragment caging in the clusters, and for distinguishing zero-KE peak from low energy fragments originating from the multiphoton processes. The H-fragment kinetic energy distributions (KEDs) were obtained from the images, and also the anisotropy parameters β were evaluated. The kinetic energy scale was calibrated with H-fragments from HBr photodissociation.³² More details about our VMI and the measurement procedures can be found in our recent publications.^{25,26}

2.2 Reflectron time-of-flight mass spectrometer

After leaving the VMI chamber the molecular beam entered a mass spectrometer chamber with RTOFMS mounted perpendicularly to the beam. This mass spectrometer offers several ionization options: electron ionization (EI) using an electron gun with 10 kHz repetition frequency and tuneable electron energy 5–90 eV with 0.7 eV resolution,^{33–35} photoionization exploiting multiphoton ionization with our tuneable UV lasers, and a special method of Na-doping and subsequent photoionization.²⁷ In the present study we used EI with 70 eV electrons. The ions were extracted perpendicularly to the beam by a 10 kV pulse and accelerated to the final kinetic energy of 8 kV. After passing the effective flight path of 0.95 m length, the ions were detected on the Photonics MCP detector in the Chevron configuration, 40 mm in diameter. The mass spectra were recorded with a resolution of $M/\Delta M \approx 5 \times 10^3$.

3 Theoretical methods

The experiments were complemented by *ab initio* calculations. The theoretical calculations were used (i) to reveal the nature of the bonding in the ethanethiol clusters, (ii) to investigate the nature of the dissociation process of the ethanethiol molecule in an excited state, considering both isolated molecules and ethanethiol clusters, (iii) to interpret the vibrational resolution of the KED spectra.

The $(\text{EtSH})_N$ ($N = 1 - 4$) clusters were optimized using the density functional approach with the B97D3 functional³⁶ and aug-cc-pVDZ basis set. The B97D3 functional includes empirical dispersion correction which is important for the present complexes. The excited states of the isolated EtSH molecule were calculated at the CASPT2/aug-cc-pVDZ level, considering the active space of 6 electrons in 7 orbitals. Two states of the A' and two states of the A'' symmetry were averaged. For the $(\text{EtSH})_2$ complex, we have used the active space of 12 electrons in 10 orbitals, using averaging over two states. Vibrational frequencies were calculated at the MP2/aug-cc-pVDZ level and scaled with a recommended factor of 0.959.³⁷

The ground state calculations (including the frequency calculations) were performed in the Gaussian09 programme,³⁸ the CASPT2 calculations were executed in the MOLPRO2012 suite of codes.³⁹

4 Results and discussion

4.1 Molecule

First, we investigated the photodissociation of isolated EtSH molecules in He-expansions. The molecular conditions were obtained at the expansion of $\approx 1\%$ EtSH (reservoir temperature $T_R = 222$ K) in $P_0 = 1$ bar of He. The example image

and corresponding KED are shown in Fig. 1 (a). A number of very similar images and mass spectra were recorded for different conditions around the above values; in particular, the reservoir temperature was increased to $T_R = 263$ K without any significant change in the results.

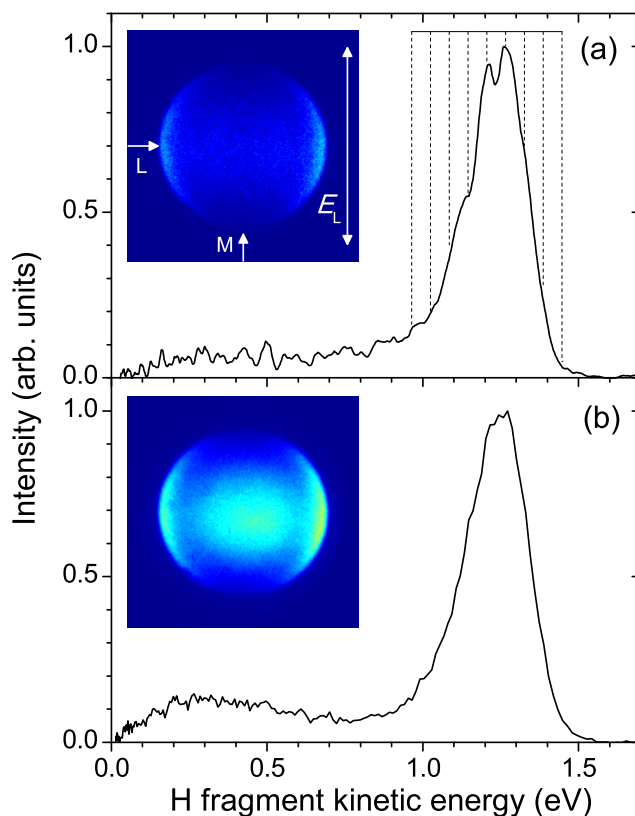


Fig. 1 (a) The H-fragment KED from EtSH molecule photodissociation at 243 nm: $P_0 = 1$ bar He, EtSH reservoir temperature $T_R = 222$ K corresponding to the concentration $C = 1.2\%$. The inset shows the raw image with the directions of the molecular (M) and laser (L) beams and the laser polarization (E_L) indicated. (b) The KED and image at an increased photon flux 8×10^{27} photons·cm⁻²·s⁻¹ illustrating the multiphoton processes.

The KED exhibits a relatively narrow peak around 1.25 eV corresponding to the fast H-fragments from the direct S–H bond fission; this is supported also by the anisotropy parameter $\beta = -1.0 \pm 0.2$ obtained by fitting the angular distribution corresponding to the fast process, which suggests an immediate dissociation after the perpendicular electronic excitation. The present image and corresponding KED in Fig. 1 (a) agree with the previous results of Zhang et al.⁶ The major difference with respect to the previous results is the resolved structure in the present KED. It ought to be mentioned, that our experiment is dedicated to cluster studies where any fine structure in the images is usually blurred by cluster effects, and therefore

the VMI setup has not been optimized for high resolution (the perpendicular arrangement is not optimal for the high resolution VMI). More than 10 images similar to the one shown in the inset in Fig. 1 (a) were recorded under comparable conditions corresponding to the isolated molecules. They were carefully analyzed, and the present KED represents the average of many spectra exhibiting the same features between ~ 0.9 eV and 1.5 eV.

The maxima at approximately 1.27 eV and 1.21 eV and the shoulder at 1.15 eV were reproduced in almost all spectra. In many spectra an additional unresolved structure with the same spacing of 0.06 eV was also observed. Therefore we tentatively indicate a series of positions within the fast fragment peak in Fig. 1 (a) with the spacing of 60 meV (484 cm^{-1}). This spacing should correspond to some vibrational levels in the EtS fragment. The observed frequency could correspond to the CH_2 wagging mode: the calculated frequency is 473 cm^{-1} or 453 cm^{-1} upon the scaling. This mode changes its frequency during the S–H dissociation (for EtSH, the frequency amounts to 782 cm^{-1}), i.e. large Franck-Condon factor is expected. Alternatively, the spacing could be attributed to the C–S stretching (681 cm^{-1}) which is, however, less probable due to the dynamical reasons.

The mass spectrum recorded under the molecular conditions is shown in ESI^+ - it corresponds to the well known mass spectra of EtSH molecule.⁴⁰ The major mass peak is the parent ion $\text{CH}_3\text{CH}_2\text{SH}^+$ at m/z 62 (M) followed by the fragments (in the order from the most to the less intense): CH_3CH_2^+ at m/z 29 (M-SH) resulting from splitting-off the SH group; CH_2SH^+ at m/z 47 (M- CH_3) resulting from splitting-off the CH_3 group; and H_2S^+ fragment at m/z 34 accompanied by fragments with $\pm\text{H}$.

4.1.1 Multiphoton processes. In the previous photodissociation study of EtSH some small fraction of slow hydrogen fragments was observed and tentatively assigned to “a different dynamical channel”.⁶ Although this slow contribution was rather negligible for $\text{C}_2\text{H}_5\text{SH}$ it was more pronounced for $\text{C}_3\text{H}_7\text{SH}$. It was argued that the corresponding process “likely occurred on the ground electronic state via internal conversion from the excited electronic state”. A small contribution due to the slow fragments similar to the previous spectra⁶ is also discernible in Fig. 1 (a). However, it was possible to obtain the KED without this contribution at low photon fluxes $\approx 1 \times 10^{27}$ photons· $\text{cm}^{-2}\text{s}^{-1}$. Some of the KEDs averaged in Fig. 1 (a) were recorded at somewhat higher photon fluxes for intensity reasons, therefore the slow fragment contribution appears there. Figure 1 (b) shows the KED with a pronounced contribution of the slow fragments recorded at a higher photon flux 8×10^{27} photons· $\text{cm}^{-2}\text{s}^{-1}$. The structure of the fast peak was smeared out, yet an unresolved shoulder structure corresponding to Fig. 1 (a) is still discernible in the KED.

The analysis of the multiphoton processes is also important since they often result in slow hydrogens near the image center: the “central blob”. However, in clusters the important information about the dissociation dynamics often appears near the center as well, e.g., the fragment caging yields a central peak. Just recently we have demonstrated that the central peak can also reveal information about interesting photochemistry: namely the H_3O radical generation in hydrogen halide photodissociation on ice nanoparticles.^{25,41,42} The present photodissociation of EtSH molecules and clusters provides an example where the different effects reflected in the image center can be disentangled, namely the multiphoton processes and the fragment caging. This will be demonstrated further below in the cluster analysis.

4.1.2 Dynamics of EtSH dissociation. The VMI experiments (KEDs and image anisotropy) suggest that the hydrogen dissociation is a direct process. The *ab initio* calculations indeed confirm this assumption: the excited state potential is purely repulsive along the S–H coordinate (see below). We further address the question whether the S–H dissociation is the only possible reaction channel. Similarly as for the methanethiol case,¹² a rupture of both the S–H and C–S bonds can in principle take place. The Potential Energy Surface (PES) is analogical to that of methanethiol, with some important quantitative differences. The two lowest excited states in the Franck-Condon region are of the A'' symmetry laying closer together than in the methanethiol case. While the C–S dissociation is accompanied with a small energy barrier on the $1A''$ state in the methanethiol,¹² both the C–S and C–H dissociation channels are open for the EtSH. This is demonstrated by Fig. 2 displaying a two-dimensional cut through the PES calculated at the CASPT2 level along the two coordinates. The PES seems rather symmetric with respect to these two coordinates. A wavepacket promoted from the ground state ($1A'$) onto the $1A''$ excited state can thus in principle split into the two possible channels, forming either the SH or H fragments. However, we need to consider the masses connected with the two coordinates, since the true dynamics is reflected rather by the PES in mass weighted coordinates. There the slope towards the C–S dissociation will diminish compared to S–H slope due to the much heavier S-atom mass compared to the mass of H. Due to these dynamical reasons, the system will follow the H-dissociation pathway which is very fast, while the SH dissociation is much slower.

4.2 Clusters

4.2.1 He-expansions. Some small clusters were generated already in He-expansions at elevated pressures $P_0 = 2$ and 3 bar and the EtSH reservoir temperature $T_R = 263$ K corresponding to the concentrations $C \approx 7.5\%$ and 5.0% , respectively. The mass spectrum shown in Fig. 3 (a) exhibits a rel-

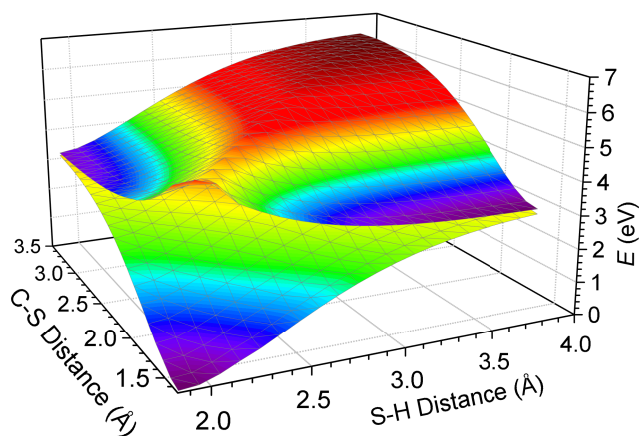


Fig. 2 The calculated PES for EtSH molecule dissociation along the S–H and C–S coordinates (see text for details).

atively strong dimer ion peak $(\text{EtSH})_2^+$ at m/z 124 (M_2) with satellites shifted by ± 1 and 2 H-atoms, $\text{EtSH}\cdot\text{SH}^+$ at m/z 95 ($M+\text{SH}$) with satellites, and even a small trimer ion $(\text{EtSH})_3^+$ at m/z 186 (M_3). It is also interesting to note that the protonated monomer $\text{EtSH}\cdot\text{H}^+$ at m/z 63 (MH) becomes larger than the EtSH^+ peak and dominates the spectrum. Also protonated hydrogen sulfide H_3S^+ at m/z 35 increases with respect to the spectrum of isolated molecules, i.e., this fragment is generated by intracluster reactions after the EI (compare to the monomer mass spectrum, Fig. S1 in ESI[†]).

This spectrum suggests that a significant amount of dimers and at least some trimers are present in the neutral beam. However, the hydrogen bonded clusters can fragment substantially upon the electron ionization,²⁷ and thus even larger clusters could be present. On the other hand, the corresponding photodissociation image shown in the inset in Fig. 3 (a) is very similar to the monomer images above. Only a very faint “central spot” can be distinguished upon a closer inspection of the image. This central spot is below recognized as the fingerprint of fragment caging in the clusters. Thus the image is dominated by the photodissociation of the monomers and free S–H bonds in the dimers and very little contribution comes from the larger clusters where the fragment caging is more probable as discussed below. The combined evidence from the mass spectra and images leads to the conclusion that the neutral beam is dominated by isolated molecules and dimers where the free S–H bonds can dissociate.

4.2.2 Ar-expansions. To generate the larger clusters, expansions in argon were exploited. The mass spectra recorded in Ar under the same conditions as He spectra above are shown in Fig. 3 (b). The series of mass peaks corresponding to the $(\text{EtSH})_n^+$ clusters up to $n = 8$ with a maximum at $n = 2$ is shown and even further peaks up to $n = 15$ are unambigu-

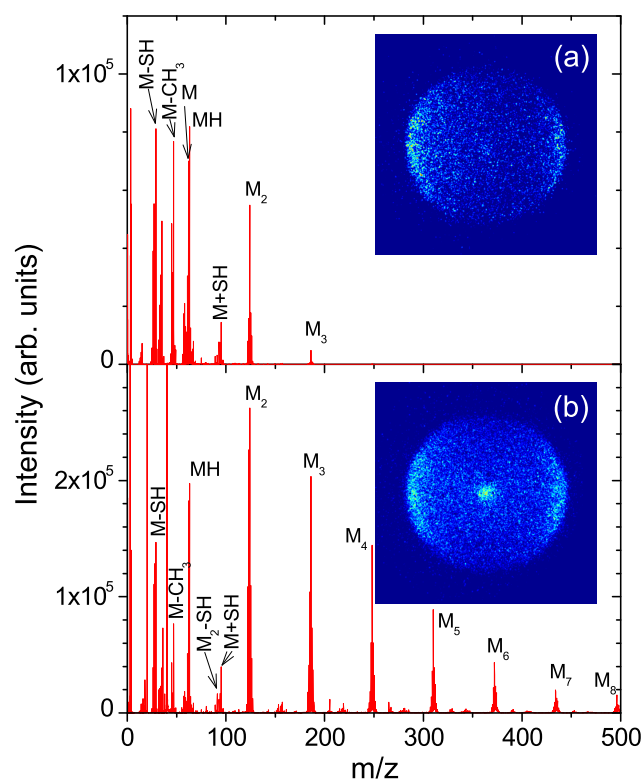


Fig. 3 The RTOFMS mass spectrum recorded in expansion of (a) $P_0 = 2$ bar He, and (b) $P_0 = 2$ bar Ar, through the EtSH reservoir at $T_R = 263$ K corresponding to the concentration $C \approx 7.5\%$. The mass peaks corresponding to the $(\text{EtSH})_n^+$ clusters are labeled. The insets show the corresponding velocity map images.

ously discernible in the spectrum. All the cluster ion peaks are accompanied by smaller satellites shifted by $\pm k\cdot\text{H}$, $k = 1-3$. The dominance of $(\text{EtSH})_n^+$ over the protonated $(\text{EtSH})_n\cdot\text{H}^+$ clusters suggests a relatively weak hydrogen bond in the clusters (compared to analogue ethanol EtOH clusters where the mass spectra are dominated by protonated $(\text{EtOH})_n\cdot\text{H}^+$ peaks⁴³). Only for $n=1$ the protonated $(\text{EtSH})\cdot\text{H}^+$ peak exceeds the monomer $(\text{EtSH})^+$ peak. There are also some minor fragments in between the major peaks corresponding to $(\text{EtSH})_n\cdot\text{SH}^+$ ($M_n+\text{SH}$) at m/z M_n+33 and $(\text{EtSH})_n\cdot\text{CH}_3\text{CH}_2^+$ ($M_{n+1}-\text{SH}$) at m/z M_n+29 . These fragments mirror the most abundant (M-SH) fragment of the monomer: the C–S bond in EtSH molecule is dissociated by EI and either the SH or CH_3CH_2 fragment remain attached to the charged cluster fragment. Thus the EI points to the C–S bond breaking in the EtSH molecule, while the UV photodissociation probes the S–H bond.

The inset in Fig. 3 (b) shows the corresponding H-fragment image which now exhibits the clear central spot corresponding to zero-KE fragments. The $(\text{EtSH})_N$ clusters generate cyclic

hydrogen bonded structures for $N \geq 3$ as shown by our calculations. In these cyclic structures the released hydrogen dissociates against the neighboring heavy S-atom and can lose part of its energy in the collision. Further inelastic collisions within the cluster eventually slow down the fragment to zero-KE. It will be shown that the KED of the *caged* fragments peaks very sharply around zero. Yet, it should be noted that the slow fragments still have to escape the cluster or the cluster has to decay in this process in order for the zero-KE fragments to be detected. Thus the *caging* for the observed fragments actually means that they are slowed down to $E_{kin} \approx 0$ eV but still released from the cluster. The calculated caging dynamics is described in the next section.

4.2.3 Cluster structure and caging dynamics. Similarly to hydrogen sulfide which possesses a weaker hydrogen bond compared to water, EtSH is less cohesive than EtOH. The enthalpy of vaporization is 27.2 kJ/mol for EtSH, which is almost two times smaller than that of the EtOH molecule (42.3 kJ/mol).⁴⁴ The EtSH vaporization enthalpy is consistent with the calculated binding energy of small EtSH clusters found in the range of 0.1-0.3 eV. Calculated structures of the complexes $(\text{EtSH})_N$ are displayed in Fig. 4. The EtSH dimer exhibits a distorted hydrogen bond arrangement which is far from collinearity. In the larger $(\text{EtSH})_N$ clusters the hydrogen bond becomes almost collinear.

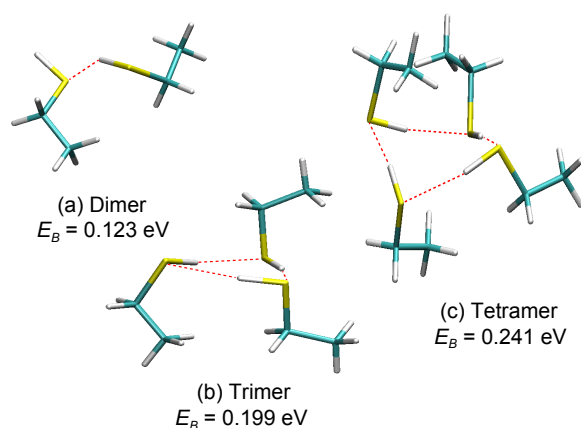


Fig. 4 The calculated structures and energetics of the small $(\text{EtSH})_N$, $N = 2-4$, clusters. E_B is the binding energy per single molecular unit (the corresponding cartesian coordinates are given in the ESI[†]).

Starting from $N = 3$, all the S–H bonds are involved in the hydrogen bonding, serving both as the hydrogen bond donors and acceptors. It is well known that the hydrogen bond in an excited state has distinctly different properties compared to the ground state.^{45,46} The effect of the neighboring molecules on the EtSH dissociation is demonstrated below in Fig. 5 where

we compare potential energy curves for the ground and excited states of the EtSH monomer and dimer. The special structure of the dimer allows us to directly compare the dissociation of the free and hydrogen bond donating S–H groups.

If we excite the EtSH unit with the free S–H bond, we observe a direct dissociation, very much like for the isolated molecules (section 4.1.2). The excess energy available upon the excitation with 5.1 eV photon estimated from this graph is in a good agreement with the KED peak maximum at 1.25 eV. On the other hand, if the hydrogen bond donating EtSH unit is excited, free dissociation is no longer possible. While the details of the potential curve depends on particular geometrical arrangement (and on the basis set used), the general trends are clear: the ground state potential energy curve is affected only very little by the presence of the solvating molecule, the excited state feels the presence of the neighboring molecule almost immediately. The potential is not dissociative in this configuration and there is much less excess energy available. However, since the free zero-KE H-fragments are observed experimentally from the clusters the dissociation of the bonding hydrogen occurs. This can be facilitated by changing the cluster geometry in the excited state, which can occur upon the UV excitation due to vibrations in the ground state. Fig. S5 in ESI[†] shows an example how the excited state PES depends on the S–H...S bond angle: a small change in the angle can yield a dissociative pathway with very little excess energy.

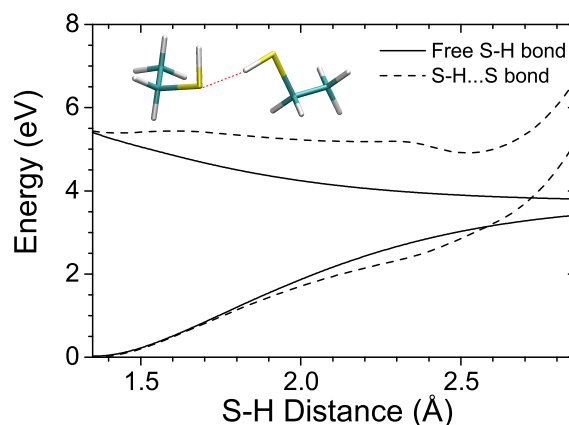


Fig. 5 The calculated PES for $(\text{EtSH})_2$ dimer dissociation along the S–H free and bound coordinates. Structure of the dimer was taken from the larger tetrameric cluster.

4.2.4 Mixed clusters. Fig. 6 (a) shows the KED and image (inset) obtained at $P_0 = 2$ bar Ar and $T_R = 276$ K corresponding to a higher EtSH concentration $C \approx 14\%$. The corresponding mass spectrum exhibits $(\text{EtSH})_n^+$ clusters up to $n = 13$ (shown in the ESI[†]). The major difference with respect to Fig. 3 (b) is that it is dominated by the monomer rather than the dimer mass peak. The images look also essentially the same

except for a higher intensity allowing for a better evaluation of the KED. Although the central peak of caged fragments is clear in the image, the zero-KE fragment contribution in the KED is negligible and the spectrum is dominated by the fast fragments similar to the fragments from isolated molecules. The fast fragments can originate from the photodissociation of the isolated unclustered molecules in the beam as well as from the *direct exit* of the H-fragments after the EtSH dissociation in the clusters.⁴⁷

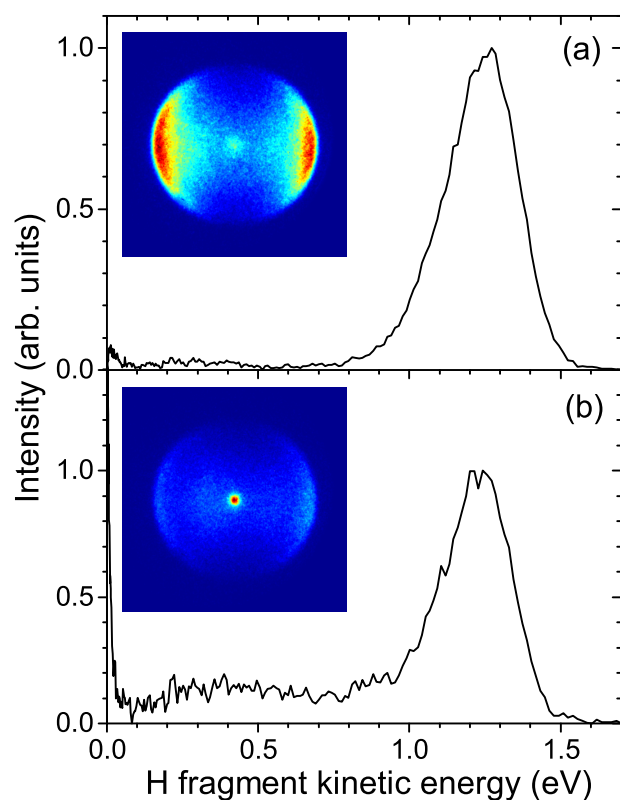


Fig. 6 The H-fragment KED recorded in the expansion of $P_0 = 2$ bar Ar through the EtSH reservoir at $T_R = 276$ K corresponding to the concentration $C \approx 14\%$ (a), and $T_R = 233$ K corresponding to $C \approx 1\%$ (b). The insets show the corresponding velocity map images.

Subsequently we tried to increase the clustering efficiency by increasing the buffer gas pressure to $P_0 = 5$ bar and then we gradually cooled down the reservoir $T_R = 276 \rightarrow 220$ K, i.e. the EtSH concentration dropped from $C = 5.6\%$ to 0.2% . The photodissociation behavior and mass spectra gradually changed and several examples are given in the ESI[†]. Fig. 6 (b) exemplifies the change in the H-fragment image and KED at $T_R = 233$ K ($C = 1.0\%$). The central peak increased in intensity and strongly dominates the image. In the corresponding KED the zero-KE maximum also exceeds the fast fragment

peak maximum by a factor of 1.4, although the zero-KE peak is very narrow (see ESI[†] for an extended part of KED near 0 eV). With further decreasing the concentration the peak of caged fragments increases with respect to the fast fragments until the spectrum exhibits essentially only the zero-KE fragments at $C = 0.2\%$.

The mass spectra (see the ESI[†]) did not change dramatically with the decreasing concentration. The essential pattern of fragments discussed above remained. As the concentration decreased from $C = 5.6\%$ to 1.8% ($T_R = 276 \rightarrow 243$ K), the observed maximum cluster fragment ion $(\text{EtSH})_n^+$ increased slightly from $n = 15$ to 17 , and then it decreased to $n = 11$ with a further decrease of the concentration to 0.2% ($T_R = 220$ K). A small but noticeable change in the mass spectra occurred around $C = 0.4\%$ ($T_R = 228$ K) where the Ar_m^+ cluster fragments start to appear with $m \leq 5$. Further below at $C = 0.3\%$ ($T_R = 224$ K) further argon clusters $m \geq 5$ occur in the spectra and additional new mixed peaks $\text{EtSH}_n \cdot \text{Ar}_m^+$, $n, m = 1, 2$ appear. This points to the generation of the mixed $\text{EtSH}_N \cdot \text{Ar}_M$ clusters.

We can combine the evidence from the mass spectra and VMI experiment to reveal some information about the size and composition of the neutral clusters:

- 1) as the EtSH concentration in argon decreases from about 1.8% ($T_R = 253$ K), the largest observed $(\text{EtSH})_n^+$ fragment size n decreases, suggesting *smaller* $(\text{EtSH})_N$ neutral precursors;
- 2) at the same time, with the decreasing concentration the zero-KE peak in VMI increases in comparison to the fast fragment peak, suggesting more fragment caging in the clusters, i.e. *larger* neutral cluster precursors;
- 3) at low concentration below 0.3% ($T_R = 223$ K) there are some mixed $(\text{EtSH})_N \cdot \text{Ar}_M$ clusters in the beam;

Apparently 1) and 2) contradict each other and the contradiction can be resolved by assuming that large mixed $(\text{EtSH})_N \cdot \text{Ar}_M$ clusters are generated at low EtSH concentrations where smaller $(\text{EtSH})_N$ clusters are encaged in larger argon “snowballs” leading to H-fragment caging. On the other hand, the weakly bound Ar atoms leave the cluster during the EI process and therefore mostly bare $(\text{EtSH})_n^+$ fragment ions occur in the mass spectra.

How large can the argon clusters be? The mean size \bar{M} of Ar_M clusters generated in nozzle expansions can be calculated from the expansion conditions (stagnation pressure, nozzle shape and temperature) using Hagena’s formula^{48,49} which has recently been outlined explicitly for our apparatus elsewhere.³⁵ This formula yields $\bar{M} \approx 50$ for the current conditions assuming pure argon expansion. At low EtSH concentrations $\leq 1\%$ the expansion is probably not perturbed significantly by the EtSH molecules and the large Ar_M clusters

can be generated. Yet, the condensation most likely starts with EtSH dimers and thus the Ar clusters will grow around the EtSH clusters. Therefore we tentatively propose that the cluster species generated at low EtSH concentrations ($\leq 1\%$) have a structure of about 50 argon atoms creating a “snowball” around about ≤ 10 EtSH molecules. It ought to be mentioned that this is in agreement with the previous experiments with hydrogen halides where for concentrations $\leq 1\%$ molecular species embedded in argon were generated, while at higher concentrations bare $(\text{HX})_N$ clusters were produced.⁴⁷

5 Conclusions

We investigated the photodissociation dynamics of S–H bond in EtSH at 243 nm. The VMI experiment was accompanied by RTOFMS after EI. The experiments were performed in various expansion regimes corresponding to species ranging from isolated molecules to dimers and large clusters of more than 10 EtSH molecules, to EtSH clusters embedded in larger Ar species. In addition, the cluster nature and photodissociation dynamics were revealed by *ab initio* calculations. From the combination of the experimental results and theory the following picture emerged for the EtSH molecule dissociation:

- The strong anisotropy of the H-fragment suggested a direct dissociation of the S–H bond. While the calculations showed purely repulsive nature of the potential energy curves along both the S–H and S–C coordinates, the dissociation channel associated with the S–C bond cleavage should be dynamically suppressed.
- The slow H-fragments observed previously⁶ were due to the multiphoton processes.
- The fast H-fragment KED reflected the vibrational excitation of the co-fragment, most likely the wagging mode of the EtS fragment.

And for the clusters the following conclusions could be drawn:

- The H-fragments were caged in $(\text{EtSH})_N$ clusters yielding zero-KE fragments beginning from the smallest clusters $N \geq 3$.
- The caging increased with the cluster size and dominated in the mixed Ar coated $(\text{EtSH})_N \cdot \text{Ar}_M$ clusters, where essentially no fast H-fragments were observed.
- The caging resulted in very sharp zero-KE H-fragments clearly discernible from the slow fragments due to the multiphoton processes.
- Our *ab initio* calculations demonstrated a very strong effect of the environment on the excited states, rationalizing the efficient caging.

The unique feature of the present experiment is the combination of the VMI in tandem with a high resolution RTOFMS. It was demonstrated that the nature of the generated clusters was reflected in the H-fragment KEDs from the VMI, as well as in the mass spectra. The complete detailed information about the clusters, their approximate size, composition and dynamics, was only revealed from the combination of the two experiments performed simultaneously on the same cluster beam, and none of these tools alone could provide the complete picture. In addition, a high level theory was necessary to fully reveal the cluster structure and photodissociation dynamics.

Acknowledgment: This work was supported by the Czech Science Foundation project Nos.: 14-14082S and 14-08937S.

References

- 1 B. J. Finlayson-Pitts and J. N. Pitts, *Chemistry of the upper and lower atmosphere*, Academic Press, San Diego, 2000.
- 2 L. Bridges, G. L. Hemphill and J. White, *J. Phys. Chem.*, 1972, **76**, 2668.
- 3 P. H. Wine, R. J. Thompson and D. H. Semmes, *Int. J. Chem. Kinet.*, 1984, **16**, 1623.
- 4 A. T. J. B. Eppink and D. H. Parker, *Rev. Sci. Instrum.*, 1997, **68**, 3477.
- 5 M. N. R. Ashfold, N. H. Nahler, A. J. Orr-Ewing, O. P. J. Vieuxmaire, R. L. Toomes, T. N. Kitsopoulos, I. A. Garcia, D. A. Chestakov, S.-M. Wu, and D. H. Parker, *Phys. Chem. Chem. Phys.*, 2006, **8**, 26.
- 6 J. Zhang, B. Jiang, X. Yang and J. Xie, *Chem. Phys. Lett.*, 2002, **364**, 80.
- 7 J. Segall, Y. Wen, R. Singer, Dulligan and C. Wittig, *J. Chem. Phys.*, 1993, **99**, 6600.
- 8 S. B. Barone, A. A. Turnipseed, T. Gierczak and A. R. Ravishankara, *J. Phys. Chem.*, 1994, **98**, 11969.
- 9 S. H. S. Wilson, M. N. R. Ashfold and R. N. Dixon, *J. Chem. Phys.*, 1994, **101**, 7538.
- 10 R. E. Stevens, C. Kittrell and J. L. Kinsey, *J. Phys. Chem.*, 1995, **99**, 11067.
- 11 L. J. Rogers, M. N. R. Ashfold, Y. Matsumi, M. Kawasaki and B. J. Whitaker, *J. Chem. Soc. faraday Trans.*, 1996, **92**, 5181.
- 12 G. A. Amaral, F. Ausfelder, J. G. Izquierdo, L. Rubio-Lago and L. Bañares, *J. Chem. Phys.*, 2007, **126**, 024301.
- 13 Z. Chen, Q. Shuai, A. T. J. B. Eppink, B. Jiang, D. Dai, X. Yang and D. H. Parker, *Phys. Chem. Chem. Phys.*, 2011, **13**, 8531.
- 14 E. Jensen, J. S. Keller, G. C. G. Waschewsky, J. E. Stevens, R. L. Graham, K. F. Freed and L. J. Butler, *J. Chem. Phys.*, 1993, **98**, 2882.
- 15 L. J. Butler, *Annu. Rev. Phys. Chem.*, 1998, **49**, 125.
- 16 B. Mouffih, C. Larrieu and M. Chaillet, *Chem. Phys.*, 1998, **119**, 221.
- 17 D. Yarkony, *J. Chem. Phys.*, 1994, **100**, 3639.
- 18 J. E. Stevens, K. F. Freed, M. F. Arendt and R. L. Graham, *J. Chem. Phys.*, 1994, **101**, 4832.
- 19 J. E. Stevens, H. W. Jang, L. J. Butler and J. C. Light, *J. Chem. Phys.*, 1995, **102**, 7059.
- 20 D. Yarkony, *J. Chem. Phys.*, 1996, **104**, 7866.
- 21 T. Bing and P. Shou-Fu, *Chin. Phys. B*, 2008, **17**, 1501.
- 22 B. G. Keyes and A. G. Harrison, *J. Am. Chem. Soc.*, 1968, **90**, 5671.
- 23 Y.-S. Cheung, C.-W. Hsu, J.-C. Huang, C. Y. Ng, W.-K. Li and S.-W. Chiu, *Int. J. Mass Spectrom.*, 1996, **159**, 13.
- 24 S. Choi, T. Y. Kang, K.-W. Choi, S. Han, D.-S. Ahn, S. J. Baek and S. K. Kim, *J. Phys. Chem. A*, 2008, **112**, 7191.
- 25 V. Poterya, J. Lengyel, A. Pysanenko, P. Svrčková and M. Fárník, *J. Chem. Phys.*, 2014, **141**, 074309.

- 26 V. Poterya, J. Kočišek, A. Pysanenko and M. Fárník, *Phys. Chem. Chem. Phys.*, 2014, **16**, 421.
- 27 J. Lengyel, A. Pysanenko, V. Poterya, J. Kočišek and M. Fárník, *Chem. Phys. Lett.*, 2014, **612**, 256.
- 28 J. Lengyel, A. Pysanenko, V. Poterya, P. Slavíček, M. Fárník, J. Kočišek and J. Fedor, *Phys. Rev. Lett.*, 2014, **112**, 113401.
- 29 M. Fárník and V. Poterya, *Front. Chem.*, 2014, **2**, 4.
- 30 B. Whitaker, *Imaging in Molecular Dynamics*, Cambridge University Press, Cambridge, 2003.
- 31 V. Dribinski, A. Ossadtchi, V. A. Mandelshtam and H. Reisler, *Rev. Sci. Instrum.*, 2002, **73**, 2634.
- 32 J. Fedor, J. Kočišek, V. Poterya, O. Votava, A. Pysanenko, L. Lipciuc, T. N. Kitsopoulos and M. Fárník, *J. Chem. Phys.*, 2011, **134**, 154303.
- 33 J. Kočišek, J. Lengyel and M. Fárník, *J. Chem. Phys.*, 2013, **138**, 124306.
- 34 J. Lengyel, R. Gorejová, Z. Herman and M. Fárník, *J. Phys. Chem. A*, 2013, **117**, 11225.
- 35 J. Kočišek, J. Lengyel, M. Fárník and P. Slavíček, *J. Chem. Phys.*, 2013, **139**, 214308.
- 36 S. Grimme, S. Ehrlich and L. Goerigk, *J. Comput. Chem.*, 2011, **32**, 1456.
- 37 NIST, *Precomputed vibrational scaling factors*, <http://cccbdb.nist.gov/vibscalejust.asp>.
- 38 M. J. Frisch, G. W. Trucks, H. B. Schlegel, G. E. Scuseria, M. A. Robb *et al.*, *Gaussian 09 Revision D*, Gaussian Inc. Wallingford CT 2009.
- 39 H.-J. Werner, P. J. Knowles, G. Knizia, F. R. Manby, M. Schütz *et al.*, *MOLPRO, version 2012.1, a package of ab initio programs*, 2012, see "<http://www.molpro.net>".
- 40 *NIST Mass Spec Data Center*, S.E. Stein, director, "Mass Spectra" in *NIST Chemistry WebBook, NIST Standard Reference Database Number 69*, ed. P. J. Linstrom and W. G. Mallard, National Institute of standards and Technology, Gaithersburg MD, 20899 (<http://webbook.nist.gov>), June 2005.
- 41 V. Poterya, M. Fárník, P. Slavíček, U. Buck and V. V. Kresin, *J. Chem. Phys.*, 2007, **126**, 071101.
- 42 M. Ončák, P. Slavíček, V. Poterya, M. Fárník and U. Buck, *J. Phys. Chem. A*, 2008, **112**, 5344.
- 43 B. D. Kay and A. W. Castleman, *J. Phys. Chem.*, 1985, **89**, 4867.
- 44 V. Majer and V. Svoboda, *Enthalpies of Vaporization of Organic Compounds: A Critical Review and Data Compilation*, Blackwell Scientific Publications, Oxford, 1985.
- 45 P. Slavíček and M. Fárník, *Phys. Chem. Chem. Phys.*, 2011, **13**, 12123.
- 46 M. Fárník, P. Slavíček and U. Buck, in *Hydrogen Bonding and Transfer in the Excited State II*, edited by K.-L. Han and G.-J. Zhao, Wiley, Chichester, UK, 2011, pp. 865.
- 47 U. Buck, *J. Phys. Chem. A*, 2002, **106**, 10049.
- 48 O. F. Hagena, *Surf. Sci.*, 1981, **106**, 101.
- 49 U. Buck and R. Krohne, *J. Chem. Phys.*, 1996, **105**, 5408.